# Novel Class of Crystal/Glass Ultrafine Nanolaminates with Large and Tunable Mechanical Properties

Francesco Bignoli,* Philippe Djemia, Giancarlo Terraneo, Gregory Abadias, Christoph Gammer, Alice Lassnig, Camila A. Teixeira, Subin Lee, Ali Ahmadian, Andrea Li Bassi, Damien Faurie, and Matteo Ghidelli*

ABSTRACT: The control of local heterogeneities in metallic glasses (MGs) represents an emerging field to improve their plasticity, preventing the propagation of catastrophic shear bands (SBs) responsible for the macroscopically brittle failure. To date, a nanoengineered approach aimed at finely tuning local heterogeneities controlling SB nucleation and propagation is still missing, hindering the potential to develop MGs with large and tunable strength/ductility balance and controlled deformation behavior. In this work, we exploited the potential of pulsed laser deposition (PLD) to synthesize a novel class of crystal/glass ultrafine nanolaminates (U-NLs) in which a ~4 nm thick crystalline Al separates 6 and 9 nm thick $Zr_{50}Cu_{50}$ glass nanolayers, while reporting a high density of sharp interfaces and large chemical intermixing. In addition, we tune the morphology by synthesizing compact and nanogranular U-NLs,

exploiting, respectively, atom-by-atom or cluster-assembled growth regimes. For compact U-NLs, we report high mass density (~8.35 g/cm^3) and enhanced and tunable mechanical behavior, reaching maximum values of hardness and yield strength of up to 9.3 and 3.6 GPa, respectively. In addition, we show up to 3.6% homogeneous elastoplastic deformation in compression as a result of SB blocking by the Al-rich sublayers. On the other hand, nanogranular U-NLs exhibit slightly lower yield strength (3.4 GPa) in combination with enhanced elastoplastic deformation (~6%) followed by the formation of superficial SBs, which are not percolative even at deformations exceeding 15%, as a result of the larger free volume content within the cluster-assembled structure and the presence of crystal/glass nanointerfaces, enabling to accommodate SB events. Overall, we show how PLD enables the synthesis of crystal/glass U-NLs with ultimate control of local heterogeneities down to the atomic scale, providing new nanoengineered strategies capable of deep control of the deformation behavior, surpassing traditional trade-off between strength and ductility. Our approach can be extended to other combinations of metallic materials with clear interest for industrial applications such as structural coatings and microelectronics (MEMS and NEMS).

KEYWORDS: *crystal/glass nanolaminates, metallic glasses, local heterogeneities, pulsed laser deposition, mechanical properties, scale-bridge structural-mechanical characterizations*
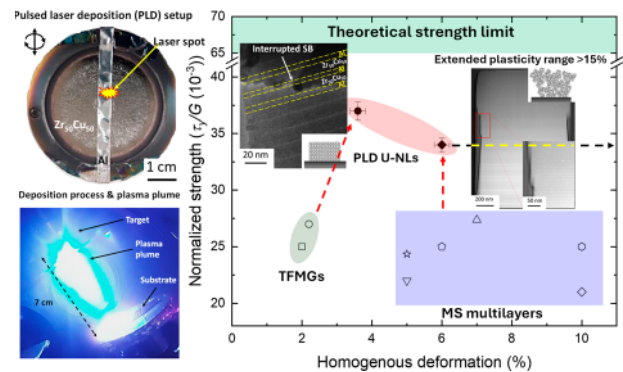
1. INTRODUCTION

Metallic glasses (MGs) are amorphous materials characterized by an atomic structure lacking long-range order leading to the combination of high yield strength (>2 GPa) and elasticity (~2%).[1] However, in their bulk form, they deform through the formation of very thin (~10 nm) shear bands (SBs), localizing the shear strain and leading to a macroscopically brittle behavior once the yield stress is exceeded.[2] To face this issue, the control of local heterogeneities at the atomic or microscale has a key role, enabling a mitigation of the SB process. A first approach is represented by the modification of the atomic arrangement through compositional segregation or by the control of free volume in order to hinder and deviate the nucleation/propagation of SBs.[3,4] As an example, ZrCu

nanoglasses[5,6] and cluster-assembled MGs[7] show a high density of amorphous interfaces, chemical fluctuations and higher free volume content, resulting in a higher yield strength (≥3 GPa) and ductility (~10%) even in tension with the formation of numerous (non-percolative) SBs that manage to accommodate the deformation.

A second strategy aims at reducing the intrinsic size of the specimen below the micrometer scale, activating mechanical size effects, resulting in homogeneous deformation because of the reduced likelihood of defects acting as stress concentrators which can trigger the SB process.[8] In this line, the synthesis of multilayers represents an interesting approach combining the layer confinement (size effects) with the possibility to control the local heterogeneities by tuning the composition/structure between the layers (i.e., amorphous and crystalline), while benefiting of a high and tunable interface density which can block SB events. For example, a Cu/ZrCu crystal/glass multilayers with a bilayer period of 20 nm deforms plastically up to 10% without formation of SBs, while still maintaining a yield strength of ∼2.4 GPa.[9] This is due to a co-deformation mechanism in which the embryonic SBs (generated in the glass layer) cannot reach the levels of stress required for nucleation/propagation due to the thickness confinement and the presence of the adjacent Cu layers, while the dislocations within Cu require more energy to propagate, overall resulting in an increment of both strength and ductility.[9,10]

However, the research on the control of local heterogeneities in MGs presents many challenges, resulting in a limited control of the SB process and the overall mechanical behavior. For instance, an easy and fast method to deposit ultrafine nanolayered structures is lacking (sublayer thickness <10 nm), enabling extensive chemical intermixing and high density of interfaces enhancing the mechanical behavior. Specifically, multilayers are usually deposited by magnetron sputtering with limitations resulting from the need of ultrafast speed for shutters opening/closing (1 cycle every 2−10 s) in combination with a fast regulation of the power applied to the targets required to produce U-NL with different composition and structures (i.e. amorphous/crystalline). Moreover, at present it is not possible to couple different nanostructuring strategies (i.e., fabrication of compact/nanogranular morphologies) within the same deposition step, preventing an advanced synthesis approach crystal/glass U-NLs with controlled microstructure and enhanced and tunable mechanical properties beyond the average of their single components together with a controlled deformation behavior.[11]

In this paper, we use pulsed laser deposition (PLD) to fabricate new $Zr_{50}Cu_{50}$/Al ultrafine nanolaminates (U-NLs) with compact or nanogranular morphologies and ultrafine bilayer periods (down to 10 nm) leading to a unique combination of strength and ductility. The local structure and mechanical properties are extensively characterized by scale-bridging techniques including X-ray diffraction/reflectivity (XRD/XRR), scanning and transmission electron microscopies (SEM/TEM), optoacoustic techniques, nanoindentation, and in situ SEM micropillar compression with post-mortem TEM to precisely investigate the effects of local heterogeneities on the strength and deformation mechanisms. Among the main results, we show that the $Zr_{50}Cu_{50}$/Al U-NLs are stronger than magnetron sputtered (MS) ZrCu-based thin film metallic glasses (TFMGs) and multilayers, reaching a yield strength of σ_y > 3.4 GPa for compact U-NLs which than fail through percolative SBs. However, cluster-assembled nanogranular U-NLs show large homogeneous deformation up to 6% (in compression), followed by the formation of superficial SBs which do not percolate through the sample even at larger deformations (>15%) as a result of the complex interplay

between the enhanced free volume within crystal/glass nanoclusters and the ultrafine nanolayered structure.

2. MATERIALS AND METHODS

2.1. Synthesis of $Zr_{50}Cu_{50}$/Al U-NLs with Controlled Bilayer Periods and Nanostructures. $Zr_{50}Cu_{50}$ (% at.) films were deposited by ablating a $Zr_{50}Cu_{50}$ target (99.99% pure, produced by Mateck), while the fabrication of $Zr_{50}Cu_{50}$/Al U-NLs was carried out by covering part of the target surface with Al (99.99% pure) stripes of different widths, as shown in Section S1. The target was ablated with a nanosecond-pulsed laser (Nd:YAG, first harmonic, λ = 1064 nm, repetition rate 10 Hz, pulse duration 5−7 ns) with a pulse energy equal to 1650 mJ, focused on the target to obtain a fluence of 14 J/cm². Si (100) was used as the substrate after being cleaned in an ultrasonic bath in isopropanol. The substrates were mounted on a rotating substrate holder with a fixed distance from the target equal to 70 mm. All depositions were performed at room temperature in vacuum (1×10^{-3} Pa) or under pure He atmosphere at a pressure of 5 Pa to deposit compact and cluster-assembled nanogranular U-NLs, respectively. The total thickness of the U-NLs is ∼800 nm, while 2 μm thick samples were deposited for micropillar compression tests.

The U-NL structures were fabricated by controlling the target roto-translation and the width of the Al stripes mounted on the $Zr_{50}Cu_{50}$ in order to tune the number of the laser shots on the ablated materials, while taking into account the difference in the deposition rates between Al and $Zr_{50}Cu_{50}$, which are, respectively, ∼2 and ∼1.1 nm/s. Specifically, 55−80 laser shots ablate the $Zr_{50}Cu_{50}$ target (corresponding to 6 and 9 nm sublayers, respectively), while a fixed number (∼20) of laser shots ablate the Al strip (corresponding to ∼4 nm sublayers). This results in U-NL with two different periods, corresponding to Al volume fractions of 30 and 40% (Section S1). TEM analyses were carried out on selected samples to precisely determine the bilayer period of $Zr_{50}Cu_{50}$ and Al. Then, a calibration was performed by combining both XRR and XRD to identify the thickness of each sublayer. This methodology has the advantage to be faster with respect to more time-consuming TEM investigations, while enabling to accurately extract the thickness of the single sublayers, as shown in Section S2. The total thickness as well as the thickness of the crystalline (t_c) and amorphous (t_a) sublayers are presented in Table 1. In this study, we focus on U-NLs with a t_a/t_c > 1, expecting a

Table 1. Crystal/Glass U-NLs Fabricated in This Work; the 800 nm U-NLs were Used for the Structural Characterization (SEM, XRD, XRR, and TEM) and Mechanical Characterization with Optoacoustic Techniques and Nanoindentation, While the 2 μm U-NLs were Used for the Micropillar Compression Tests

	total thickness 800 nm	total thickness 2 μm
nanolayer period [nm $Zr_{50}Cu_{50}$/nm Al]	800/0, 6/4, 9/4	9/4

high strength due to the larger fraction of amorphous phase, while keeping a high plasticity due to the presence of FCC Al sublayers, as found from molecular dynamics simulations[12] and observed in ZrCu/Cu 100/50 nm multilayers (t_a/t_c = 2) reporting a combination of a yield strength (σ_y) of 2.1 GPa and ductility around 12%.[10]

2.2. Structural Characterization. The crystallographic structure of the U-NLs was investigated by X-ray diffraction (XRD) using a θ-2θ Bruker D8 Advanced system with Cu Kα radiation (λ = 0.154 nm) operated in grazing incidence geometry with an incidence angle of 0.95° and a 2θ scan range of 20−90°. Data were acquired overnight by a Lynx Eye detector in continuous scanning mode with a 2θ step size of 0.14°.

A field emission SEM (Supra, Zeiss) 40 equipped with a Bruker energy dispersive X-ray spectrometer (EDX) was used to perform morphological and elemental characterization of the U-NLs deposited on Si (100) substrates.
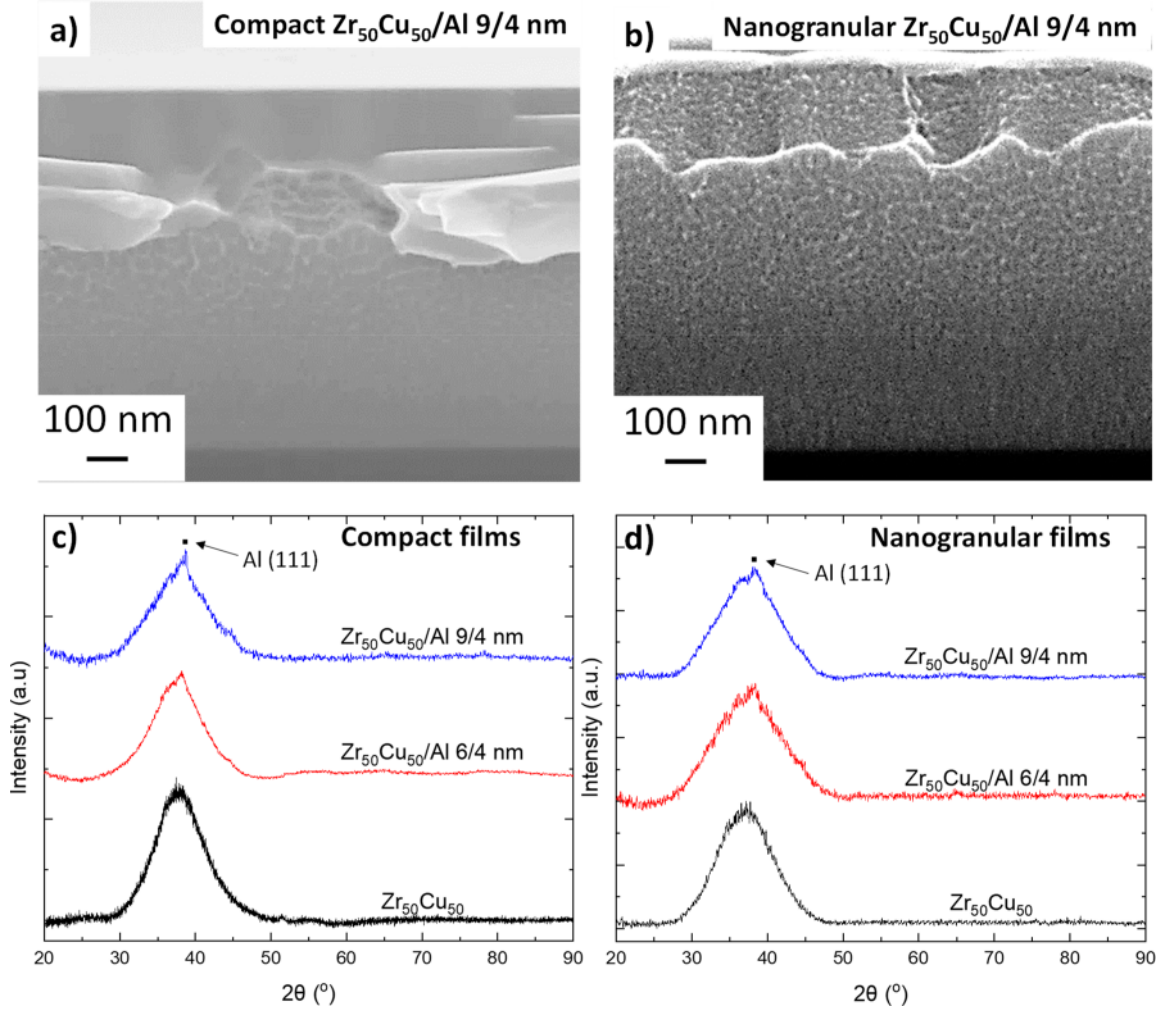
Figure 1. Cross-sectional SEM and XRD patterns as a function of the bilayer period of compact (a and c) and nanogranular (b and d) $Zr_{50}Cu_{50}$/Al U-NLs, respectively.

X-ray reflectivity (XRR) scans were obtained with a Seifert XRD 3000 diffractometer operating at 40 kV and 40 mA using a Cu Kα source. The scans were carried out between 0.2° and 2.2° with a step of 0.05° to determine the density of the U-NLs and estimate the period of the NL structure structures, as explained in Section S2.

To get high resolution information on the layered structures and elemental distribution of the as deposited nanolayered structures, cross-sectional transmission electron microscopy (TEM) analyses were performed using a JEOL 2200 FS instrument operating at 200 kV. A combination of high-angle annular dark-field scanning TEM (HAADF-STEM), selected area electron diffraction (SAED), and STEM-EDX were acquired to characterize the morphology structure and chemistry at the nanoscale. The lamellae used for TEM characterization were prepared with a Ga focused ion beam (FIB) with an extremely low current equal to 50 pA, while protecting the sample with a 100 nm Pt layer to minimize damage.

For the post-mortem characterization of the tested pillars, TEM and STEM-EDX were carried out in an aberration probe-corrected Thermo Fisher Titan Themis 60−300 equipped with the Chem-iSTEM Super X EDX detector operated at 300 kV.

2.3. Mechanical Characterization. The elastic properties of the U-NLs were extracted by Brillouin light scattering (BLS) spectroscopy and picosecond laser ultrasonics in air, as described in Section S3 and in the references.[13,14]

The Young's modulus (E) and the hardness (H) of the U-NLs were extracted by nanoindentation by using a KLA G200 with a Berkovich diamond indenter operated in continuous stiffness measurement (CSM) mode to measure their depth profile. A standard fused silica

sample was tested before and after the measurements for tip and frame stiffness calibrations. The Oliver and Pharr[15] model was applied to extract E and H at indentation depths equal to 10% of the film thickness with a fixed load rate of 0.05 s^{-1}, a thermal drift of <0.05 nm/S, and 25 indents for each sample. More details can be found in Section S4.

Micropillar compression tests were performed on the 2 μm samples in a SEM (Merlin Gemini II, Zeiss) with a Bruker Hysitron PI89 SEM PicoIndenter (maximum force of 0.5 N and noise floor of 5 μN) equipped with a 2 μm diamond flat punch (Synthon-MDP AG) in displacement control mode with a strain rate of 10^{-2} s^{-1}. Micropillars were machined with a gallium focus ion beam (FIB, Crossbeam 550L Zeiss) operated at an acceleration voltage of 30 kV using a three-step process: coarse milling with a current of 7 nA, 1.5 nA for intermediate, and 300 pA for fine milling. Four pillars were tested for each sample with stress obtained as the force divided by the top area of the pillar. The pillars have an average diameter of 720 nm and height around 2 μm to avoid substrate interferences and the activation of mechanical size effects, which increase extrinsically the yield strength and ductility of the MGs when the diameter of the tested samples goes below 300 nm.[16,17] More details regarding the tests and how the yield strength σ_y and homogeneous deformation with their statistics were obtained can be found in Section S5.

3. RESULTS AND DISCUSSION

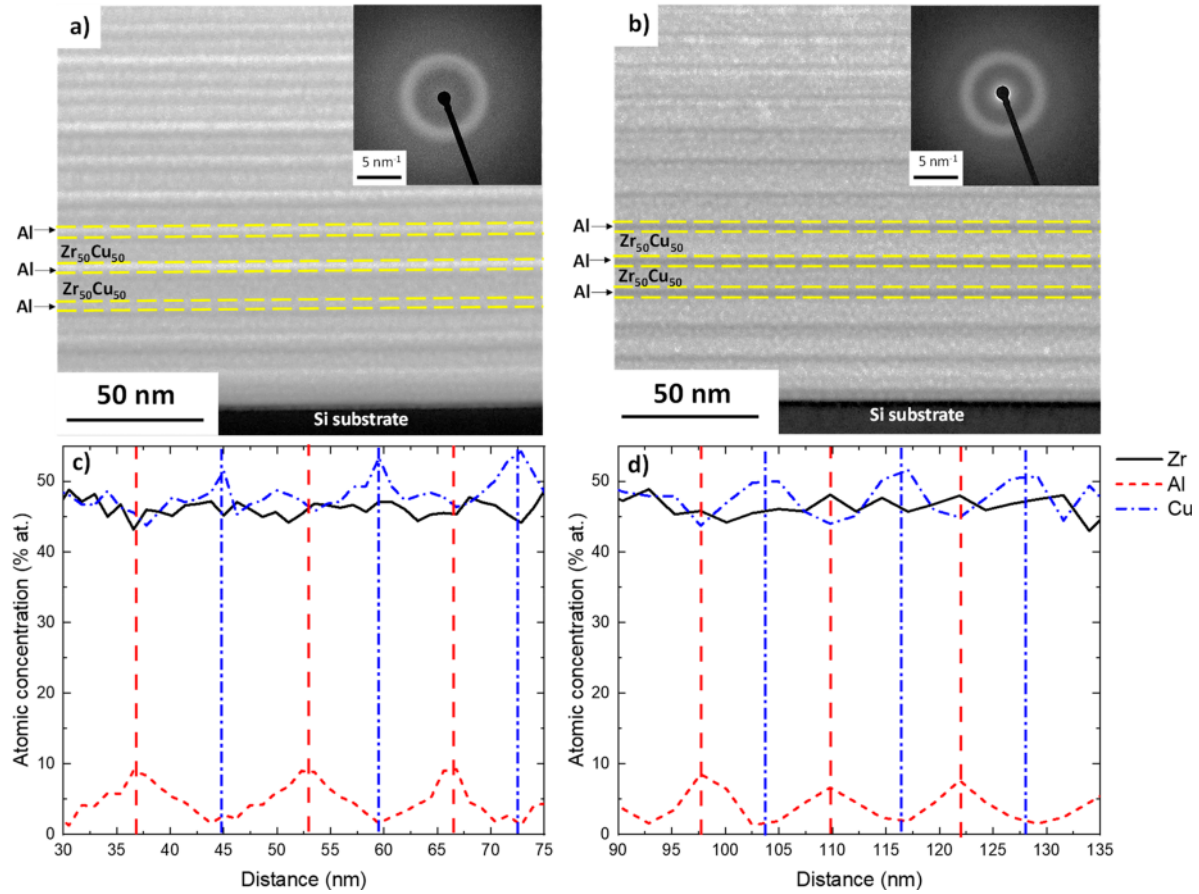**3.1. Atomic and Microstructure of $Zr_{50}Cu_{50}$/Al U-NLs.** The microstructure of compact U-NLs deposited in vacuum

Figure 2. HAADF-STEM images of compact (a) and nanogranular (b) $Zr_{50}Cu_{50}$/Al U-NLs showing the nanolayered microstructure with a $Zr_{50}Cu_{50}$ layer thickness of 9.0 ± 0.5 separated by 4.0 ± 0.5 nm Al layers. The corresponding SAED patterns in the insets of (a) and (b) highlight mainly the amorphous structure of both samples. The averaged STEM-EDX line profiles across several layers for both compact (c) and nanogranular (d) U-NLs show a extensive intermixing between the nanolayers.

and of nanogranular U-NLs deposited at 5 Pa He has been investigated by SEM, XRD, and TEM. The SEM cross-section (Figures 1a and 1b) displays the absence of macroscopic defects such as porosities and phase segregations, which could affect the mechanical behavior, while showing the presence of corrugations, induced by the propagation of SBs typical of MGs.[18] This is expected since the t_a/t_c is >1, leading to a deformation process dominated by SBs propagation especially when performing cleavage forcing sharp crack propagation from the Si substrate to the U-NLs.[12,18]

The XRD patterns for the compact and nanogranular $Zr_{50}Cu_{50}$/Al U-NLs presented in Figures 1c and 1d, respectively, show that the pure $Zr_{50}Cu_{50}$ is completely amorphous with a main peak centered at $2\theta = 37.7°$, as expected from the literature.[14] However, the full width at half-maximum (fwhm) of the nanogranular film in Figure 1d is wider (10°) than that of the compact film counterpart in Figure 1c (7.5°), indicating a more disordered and heterogeneous structure due to their cluster-assembled growth similar to nanoglasses.[7,19] The U-NLs also show a peak at $2\theta = 38.5°$, which corresponds to the (111) plane of FCC Al, indicating a textured growth of the crystalline layer. The peak is more pronounced with an increased Al relative fraction. The size of the Al crystallites, obtained by Scherrer's equation on the Al (111) reflection, is ~4.0 ± 0.5 nm; see Section S2 for more information.

A more detailed investigation of the nanostructure of the U-NLs alternating 4.0 ± 0.5 nm of Al and 9.0 ± 0.5 nm of $Zr_{50}Cu_{50}$ (referred as $Zr_{50}Cu_{50}$/Al 9/4 nm) was conducted by STEM. Figures 2a and 2b display HAADF STEM images of compact (a) and nanogranular U-NLs (b), revealing a nanolayered structure with straight interfaces. Such structure differs from previously reported nanolaminates with similar bilayer periods (6−20 nm) deposited by magnetron sputtering, which usually possess undulating interfaces due to the incomplete coalescence of the islands during the sputtering of the single interlayers.[11,20,21] As a matter of fact, PLD enables larger energy of the deposited species (>15 eV) vs magnetron sputtering (~1 eV), allowing a faster percolation of the islands, forming the defined interlayers with large chemical intermixing.[22] Figure 2b also shows that the single layers composing the nanogranular U-NLs are not homogeneous, but formed by nanosize clusters due to the in-plume cluster formation induced by the background deposition pressure.[7] These clusters have brighter cores and darker surroundings, indicating a change in the relative density from the center (denser) to the interfaces (less dense) due to chemical segregation during the cluster formation and the formation of topological defects during the bonding of adjacent clusters such as in nanoglasses.[5,6] SAED patterns in the insets of Figures 2a and 2b reveal a single band in agreement with the XRD, but without spot patterns expected from the crystalline Al layers. This could be related to the elemental chemical intermixing

phenomena (formation of the ZrCuAl) for both compact and nanogranular U-NLs (Figures 2c and 2d) as well as the difficulty to obtain SAED patterns of the nanocrystalline Al, which possesses very small intrinsic sizes (≤ 4 nm). The thickness of the layers estimated by HAADF STEM and STEM-EDX line profiles are quite similar and can be considered equal. In both cases, we show chemical intermixing between the Al and the $Zr_{50}Cu_{50}$ layers with high concentrations of Zr and Cu in the Al layers and with the peaks of Al concentrations (dash vertical lines) being in counterphase with the Cu concentration (dash−dot vertical lines) due to the low miscibility between Al and Cu ($\Delta H_{mix\ Al-Cu} = -1$ kJ/mol).[23] The intermixing between the layers is favored by the thin thickness of the sublayers of the U-NLs,[11,24] the high mixing enthalpy between Zr and Al ($\Delta H_{mix\ Zr-Al} = -44$ kJ/mol),[23] the high reactivity of the Al nanocrystalline grain boundaries,[25] and the high surface mobility of the atoms during the film growth due to the high energies of PLD.[22] This chemical diffusion of Al and ZrCu between the different sublayers generates a ZrCuAl phase with an interatomic distance close to $Zr_{50}Cu_{50}$ (2.5 Å).[13] However, a more accurate analysis by using atom probe tomography (APT) will be necessary to achieve higher spatial resolution, especially for the case of U-NLs with nanometer-sized bilayer periods explored in this study. The SAED signal of the ZrCuAl phase reduces the intensity of the diffraction signal of the base components (ZrCu and Al) such as in TiAl intermetallics grown during the annealing of Al/Ti multilayers,[26] while slightly decreasing the effective thickness of the crystalline layer (t_c), consequentially increasing the t_a/t_c ratio, which, however, remains >1. This results in comparable mechanical properties and deformation behavior.[12]

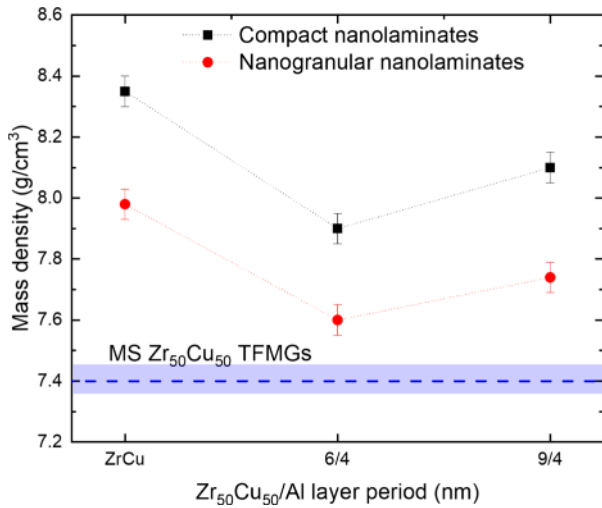Figure 3 shows the evolution of the mass density for U-NLs compared to magnetron sputtered (MS) deposited ZrCu

Figure 3. Evolution of the mass density of compact and nanogranular $Zr_{50}Cu_{50}$/Al U-NLs with different layered structures.

films.[13,27] First, the nanogranular U-NLs are slightly less dense than their compact counterparts due to the higher amount of free volume originated by the cluster-assembled growth.[7] Moreover, the density of compact $Zr_{50}Cu_{50}$ PLD films (8.35 g/cm^3) is at least 10% higher than their traditional MS counterparts (7.4 g/cm^3).[13,27] This phenomenon, already observed in the literature for oxides[28] and carbon films,[29] is

related to the high fluence (energy per unit area) used in PLD, which confers higher amounts of kinetic energy to the atoms in the plasma plume, allowing the growth of films with an enhanced closely packed atomic structure.[22] Lastly, for both compact and nanogranular nanolaminates, the mass density decreases increasing the Al volume fraction (a) varying from 8.35 and 7.98 g/cm^3 for compact and nanogranular $Zr_{50}Cu_{50}$ down to 7.9 and 7.6 g/cm^3 for the corresponding U-NLs alternating 4 nm of Al and 6 nm of $Zr_{50}Cu_{50}$. However, such values are still higher than the density of MS $Zr_{50}Cu_{50}$ with 7.4 g/cm^3 even considering a 40% Al vol. fraction within the PLD-deposited U-NLs. This can be explained by the high energies of PLD and high chemical intermixing between the Al and $Zr_{50}Cu_{50}$ layers forming a denser ZrCuAl amorphous phase (~ 7.1 g/cm^3).[13,27,30]

3.2. Mechanical Properties of $Zr_{50}Cu_{50}$/Al U-NLs. Figure 4 presents the evolution of the Young's modulus (E) obtained by optoacoustic techniques and the nanoindentation and hardness (H) obtained by nanoindentation. Both compact and nanogranular U-NLs follow the same trend and have similar values of E and H as a function of the layer period, indicating that the transition from compact to nanogranular morphology has only a minor effect on the elastic properties of the U-NLs. This is probably related to the fact that elastic constants are essentially linked to structure (at the bond scale) rather than microstructure. The small (7%) difference between the elastic modulus measured by nanoindentation and optoacoustic techniques is related to substrate effects present during nanoindentation[31] and have already been observed in other works.[13,14] Furthermore, we observe that the E and H of our PLD-deposited films are much higher (30%) than those of sputter-deposited ZrCu TFMGs[14,32] and similar multi-layers.[9,10] This results from the higher density of the PLD films as observed in the W and W−O films deposited with different densities by Besozzi et al.,[33,34] in which the increase of the elastic moduli is directly proportional to the densification of the films.

The introduction of the Al nanolayering increases E and H from 120 and 8.6 GPa of $Zr_{50}Cu_{50}$ up to 139 and 9.3 GPa for the corresponding U-NLs with $Zr_{50}Cu_{50}$/Al 9/4 nm. These values are higher than the theoretical average of E and H of the single $Zr_{50}Cu_{50}$ and Al layers based on the relative volume fraction of Al, namely 105 and 6.4 GPa, because of the formation of a U-NL structure. However, such trend is opposite to what is observed in the literature of crystal/glass multilayers reporting the decrement of H for larger fractions of the FCC crystalline phase such as in the case of ZrCu/Cu multilayers, which show a reduction of H down 5.9 GPa for a 50% Cu volume fraction.[10,35] The behavior observed of U-NLs can be related to a combination of many factors, including the high density of crystal/glass interfaces, which have been demonstrated to increase the mechanical strength of the structure[24] confining and deviating the propagation of SBs, while increasing the stress necessary for plastic deformation.[36] A second factor to be considered is the large chemical intermixing with the formation of a ZrCuAl phase involving the formation of strong Zr−Al and Cu−Al bonds and the creation of short-range order Al-centered polyhedral clustered structures, providing high strength as well as a delay to the propagation of SBs.[13,37] To sum up, the formation of the ZrCuAl phase and the ultrafine nanolayered structure reinforces the overall mechanical properties, despite the
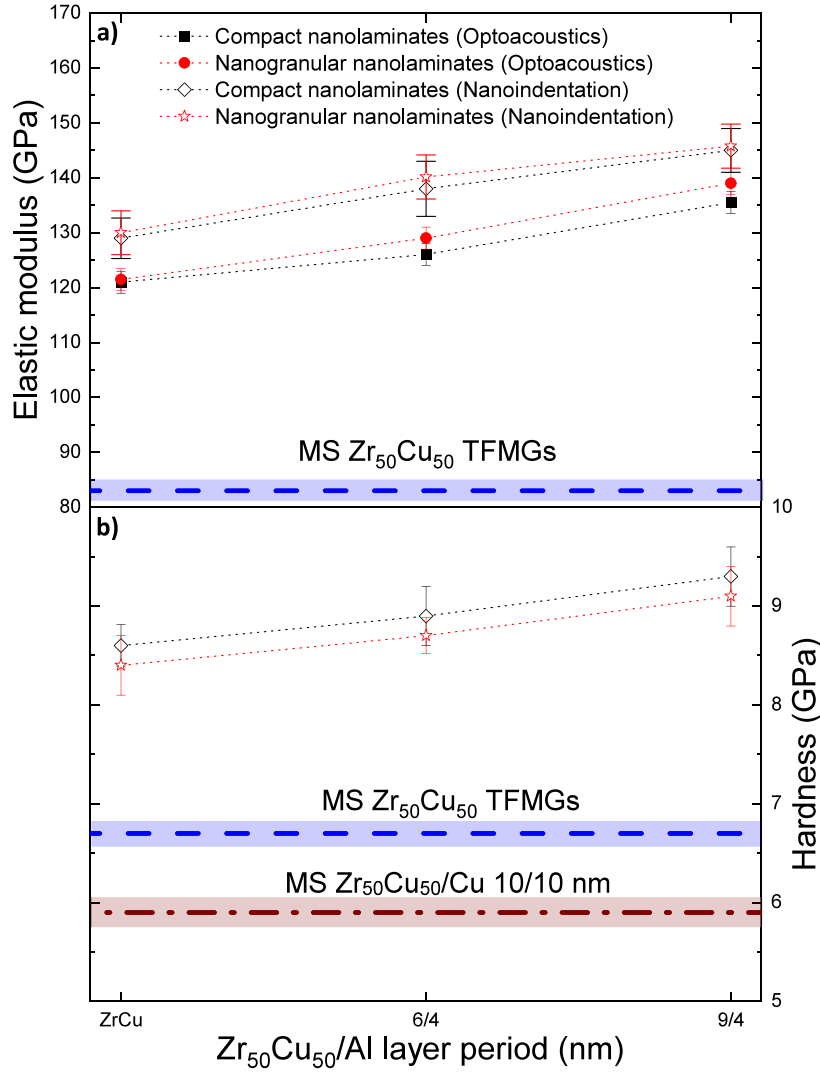
Figure 4. Evolution of the elastic modulus (a) and hardness (b) of compact and nanogranular $Zr_{50}Cu_{50}/Al$ U-NLs for different U-NL configurations. Data are compared with traditional MS ZrCu and ZrCu/Cu multilayers.

presence of an Al phase, with low E and H values equal to 69 and 1.5 GPa, respectively.[38]

Micropillar compression tests were carried out on both compact and nanogranular $Zr_{50}Cu_{50}/Al$ 9/4 nm U-NLs which had the highest density and H (Figures 3 and 4), thus expecting higher plasticity. Moreover, the higher fraction of ZrCu (vs the $Zr_{50}Cu_{50}/Al$ 9/4 U-NLs) is expected to provide enhanced mechanical size effects,[8] while the presence of crystalline Al will have beneficial SB booking effects. For the compact U-NLs, Figure 5a shows that after the elastic behavior reaches up to 3.3%, the stress–strain curve is interrupted by the propagation of the first SB (the full stress–strain curve and additional data/images are reported in Section S5). The yield stress (σ_y) is equal to 3.60 ± 0.08 GPa, which is 1.1 GPa higher than of MS-deposited ZrCu homogeneous TFMGs and of ZrCu crystal/glass multilayers,[9,39] as a result of the high mass density of the PLD U-NLs, significant chemical intermixing, and the large density of crystal/glass interfaces.[24] The first SB starts to appear at 3.60 ± 0.22% strain, a value significantly larger than the monolithic TFMG threshold which is usually around 2%.[40,41] This improvement of plasticity is connected to the presence of Al layers, which confine and block the SBs in the amorphous ones, promoting a more homogeneous

deformation. This is confirmed in Figures 5b and 5c reporting the *post-mortem* SEM and TEM images of the micropillar, highlighting the SB blocking effect of Al-rich layers, while showing the nanoscale periodicity of the Al and $Zr_{50}Cu_{50}$ layers (Figure 5d). The formation of through-the-specimen percolative SBs occurring in U-NLs is also expected since the t_a/t_c (thickness of amorphous layer/thickness of crystalline layer) ratio is >1, showing a dominant fraction of amorphous sublayers. As a matter of fact, molecular dynamic simulations show that if $t_a/t_c > 1$, the deformation by nucleation and propagation of SB is predominant with respect to the grain boundary and dislocation plasticity of the crystalline sublayer.[12] For this reason, the compact U-NLs fail mainly by SB events, while the chemical heterogeneities and high density of interfaces manage to block and delay their propagation leading to an increment of the yield strength in combination with a a modest increase of the overall plasticity which is however ~40% higher with respect to monolithic TFMGs (~2%).[42]

Figure 6 shows a representative stress–strain curve in compression of the nanogranular $Zr_{50}Cu_{50}/Al$ 9/4 nm U-NLs and corresponding *post-mortem* SEM and TEM images (the raw stress–strain curve and additional data/images are
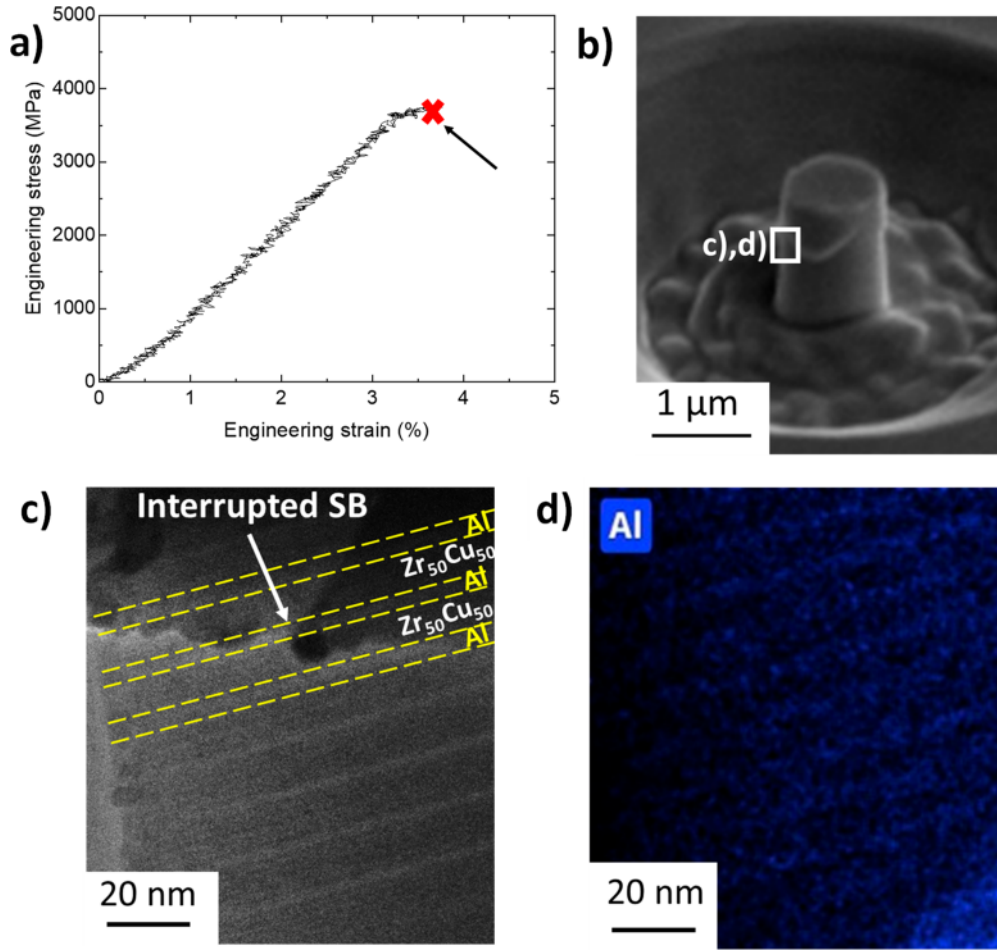
Figure 5. (a) Engineering stress vs engineering strain curve of compact $Zr_{50}Cu_{50}/Al$ 9/4 nm U-NLs with a black arrow highlighting the formation of the first SB causing brittle failure. (b−d) *Post-mortem* SEM, TEM, and EDX-STEM cross-sections of the micropillar showing SB blocking at Al layers.
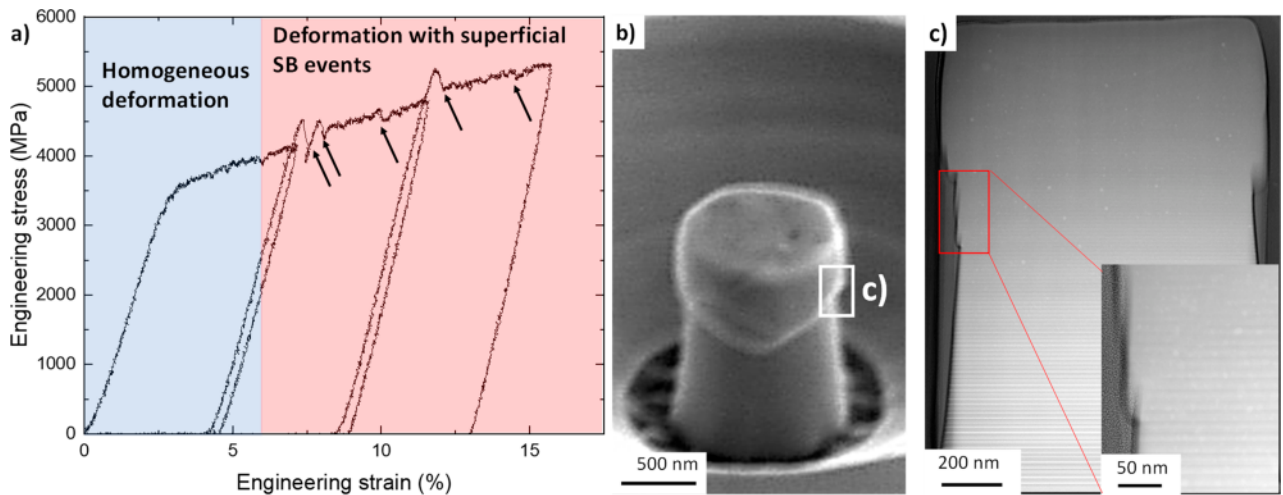

Figure 6. (a) Engineering stress−strain curve of nanogranular $Zr_{50}Cu_{50}/Al$ 9/4 nm U-NLs highlighting the different deformation regimes (homogeneous and with superficial SB events underlined by black arrows). (b and c) *Post-mortem* SEM image of the micropillar and HAADF-STEM cross-section, highlighting superficial non-percolative shear bands.

reported in Section S5). The stress increases linearly up to 2.5% deformation, upon which the pillar yields at $\sigma_y \approx 3.40 \pm 0.06$ GPa, a value slightly below the compact counterpart (Figure 5) and in agreement with the trend of hardness (Figure 4b). This is related to the higher amount of free volume of cluster-

assembled U-NLs, which activates plastic deformation at lower stresses and strains with respect to the more ordered compact U-NLs.[43,44] However, the nanogranular U-NLs show homogeneous deformation up to $6.00 \pm 0.36\%$, and then SBs start to appear on the surface of the micropillar as revealed by TEM
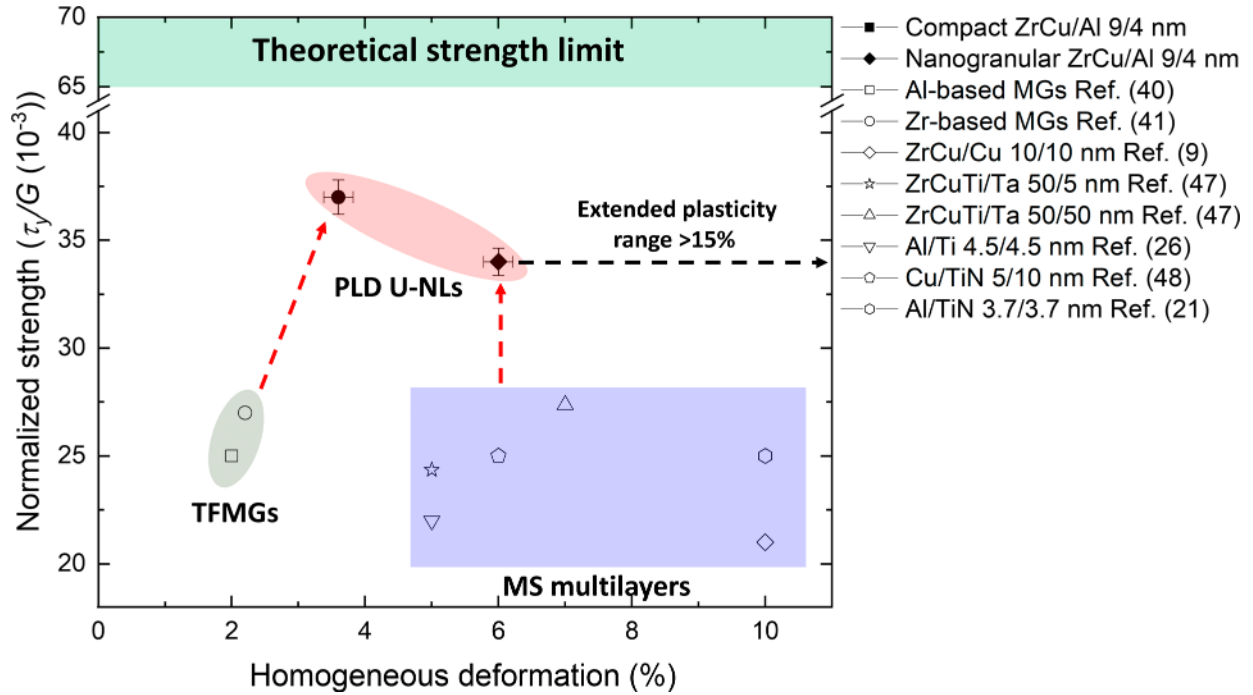
Figure 7. Map of the normalized strength vs homogeneous deformation comparing PLD U-NLs with traditional MGs and crystal/glass multilayers fabricated by magnetron sputtering (MS), as reported in the literature. A black dashed arrow indicates the interval of extended plasticity of the nanogranular U-NLs in which only superficial nonpercolative SBs appear.

observations (Figure 6c). However, these events are not followed by a percolation even at larger deformations (>15%), as shown in Figure 6b,c, in which only some superficial SB are found. This phenomenon is similar to the one observed in nanoglasses in the literature,[6,17] in which the large amount of free volume between amorphous clusters prevents the percolation of embryonic SBs in a single major event such as in traditional MGs,[43,44] while favoring a pseudohomogenous deformation through the propagation of fine SBs, which are confined in the external surface.[6] Similar deformation mechanisms are also reported for the CoCrNi/TiZrNbHf 18/12 nm crystal/glass multilayers which could achieve σ_y values of ~3.6 GPa and large plasticity (up to 15%) with nonpercolative cracking events as observed in nanogranular U-NLs (Figure 6) due to the high density of interfaces and chemical partitioning between the two sublayers, managing to block crack percolation.[45]

Figure 7 reports the normalized shear strength τ_y/G (G = shear modulus) vs homogeneous deformation for different classes of materials. τ_y is calculated as $\sigma_y/2$,[46] while G is obtained by BLS for the U-NLs (Section S3) or as $E/(2(1 + \nu))$, in which ν is the Poisson's ratio from literature data. We compared our data with homogeneous TFMGs,[40,41] MS multilayers with a similar bilayer period alternating crystal/glass sublayers,[9,47] fully crystalline metallic NLs,[26] and crystalline metal/ceramic NLs.[21,48]

We show that the PLD U-NLs have very high τ_y/G values equal to 37×10^{-3} for compact U-NLs and 34×10^{-3} for the nanogranular U-NLs, which are roughly half the theoretical strength limit $(1 + \nu)/20$ ($\nu = 0.3-0.4$) obtained from the theoretical yield strength σ_{th} equal to $E/20$ for metallic materials.[49] Such values are significantly higher than those of current MS multilayers and TFMGs reported in literature as a result of the high mass density (originated by the high plasma energies of PLD) and the fine nanolayered structure with large

density of nanointerfaces, enabling to increase the stress required for the propagation of SBs. These interfaces confine and deviate the SBs generated within the glassy layers, while absorbing the dislocation propagating within the crystalline ones. Finally, the nanogranular U-NLs possess the best combination of normalized strength and homogeneous deformation combining the inter-layer chemical heterogeneities and the intra-layer density fluctuations related to the cluster assembled growth, preventing the propagation of mature SB events. Moreover, the high free volume fraction (originated by the cluster-assembled growth) and the complex interplay with the local heterogeneities (nanointerfaces and chemical fluctuations) provide the formation of non-percolative SB events which are arrested in the proximity of the surface even at larger (>15%) deformations, thus potentially extending the field of applicability of such materials way above MS multilayers.

4. CONCLUSIONS

In this work, we push the limits of pulsed laser deposition (PLD) to develop crystal/glass (Al/$Zr_{50}Cu_{50}$) ultrafine nanolaminates (U-NLs) with controllable nanometer-scale bilayer periods and tunable (compact and nanogranular) morphology. We show the following:

- Both compact and nanogranular U-NLs are characterized by a fine nanolayering alternating ~4 nm Al with 6–9 nm $Zr_{50}Cu_{50}$ sublayers. This results in a high density of crystal/glass interfaces, coupled with significant interlayer chemical intermixing with the formation of a ZrCuAl phase.

- The mass density of the U-NLs is larger than monolithic ZrCu metallic glasses, despite the addition of Al (~30–40% vol.). This is attributed to the high kinetic energy of the ablated species during the PLD process, leading to

densification and chemical intermixing promoted by the high out-of-equilibrium conditions.

- The unique microstructure of U-NLs results in significantly enhanced E and H values, reaching up to 139 and 9.3 GPa, respectively which are 30% above literature as a result of the high density of nano-interfaces, the larger mass density, and the formation of a ZrCuAl phase, increasing the stress necessary for SB propagation and improving the mechanical properties.

- Micropillar compression tests reveal that compact U-NLs exhibit the highest yield strength (σ_y) of ~3.6 GPa. However, the deformation involves the propagation of SBs, which are partially mitigated by the Al-rich layers, resulting in failure ~3.6% deformation. In contrast, nanogranular U-NLs have slightly lower σ_y of ~3.4 GPa, but their higher free volume content and enables to accommodate more extensive homogeneous elasto-plastic deformation, without catastrophic failure even for deformations >15%.

- Our crystal/glass U-NLs demonstrate a superior balance between normalized strength τ_y/E and ductility, surpassing the majority of multilayers and monolithic TFMGs reported in the literature. Additionally, we show the absence of percolative SBs in nanogranular U-NLs, expanding their range of applicability way beyond that of sputter-deposited MLs.

Overall, we demonstrate the effective manipulation of atomic and microstructural heterogeneities within ultrafine crystal/glass (Al/$Zr_{50}Cu_{50}$) nanolaminates as a successful approach to finely tune and enhance the mechanical properties beyond the single-phase constituents, surpassing the traditional tread-off between strength and ductility. Our findings offer crucial insights for the design of new metallic thin films with exceptional mechanical performances capable of resisting intense and complex loading configurations, which are relevant across various application domains such as microelectronics and structural coatings.

■ AUTHOR INFORMATION

Corresponding Authors

Francesco Bignoli − *Laboratoire des Sciences des Procédés et des Matériaux (LSPM), CNRS, Université Sorbonne Paris Nord, 93430 Villetaneuse, France; Dipartimento di Energia, Laboratorio Materiali Micro e Nanostrutturati, Politecnico di Milano, I-20133 Milano, Italy;* orcid.org/0009-0006-2844-3147; Email: francesco.bignoli@lspm.cnrs.fr

Matteo Ghidelli − *Laboratoire des Sciences des Procédés et des Matériaux (LSPM), CNRS, Université Sorbonne Paris Nord, 93430 Villetaneuse, France;* orcid.org/0000-0001-6057-9040; Email: matteo.ghidelli@lspm.cnrs.fr

Authors

Philippe Djemia − *Laboratoire des Sciences des Procédés et des Matériaux (LSPM), CNRS, Université Sorbonne Paris Nord, 93430 Villetaneuse, France*

Giancarlo Terraneo − *Laboratory of Supramolecular and Bio-Nanomaterials (SupraBioNanoLab), Department of Chemistry, Materials, and Chemical Engineering "Giulio Natta", Politecnico di Milano, 20131 Milano, Italy;* orcid.org/0000-0002-1225-2577

Gregory Abadias − *Institut Pprime, UPR 3346, CNRS-Université de Poitiers-ENSMA, 86073 Poitiers Cedex 9, France*

Christoph Gammer − *Erich Schmid Institute of Materials Science, Austrian Academy of Sciences, 8700 Leoben, Austria;* orcid.org/0000-0003-1917-4978

Alice Lassnig − *Erich Schmid Institute of Materials Science, Austrian Academy of Sciences, 8700 Leoben, Austria;* orcid.org/0000-0001-6471-1635

Camila A. Teixeira − *Institute for Applied Materials, Karlsruhe Institute of Technology, 76344 Eggenstein-Leopoldshafen, Germany*

Subin Lee − *Institute for Applied Materials, Karlsruhe Institute of Technology, 76344 Eggenstein-Leopoldshafen, Germany;* orcid.org/0000-0002-4629-8004

Ali Ahmadian − *INT Institute of Nanotechnologies, Karlsruhe Institute of Technology, 76344 Eggenstein-Leopoldshafen, Germany*

Andrea Li Bassi − *Dipartimento di Energia, Laboratorio Materiali Micro e Nanostrutturati, Politecnico di Milano, I-20133 Milano, Italy;* orcid.org/0000-0002-1265-4971

Damien Faurie − *Laboratoire des Sciences des Procédés et des Matériaux (LSPM), CNRS, Université Sorbonne Paris Nord, 93430 Villetaneuse, France;* orcid.org/0000-0001-7259-3958

Author Contributions

F.B.: carried out the PLD deposition, SEM and XRR, and optoacoustic and nanoindentation experiments and assisted with micropillar compression. He analyzed all the data and wrote the original draft. G.A.: supervised the XRR characterization. A.L. and C.G.: carried out the TEM experiments. A.A.: carried out the TEM experiments on micropillars after compression. C.A.T.: fabricated and compressed the micropillars. S.L.: supervised the micropillar compression experiments and reviewed the corresponding data. G.T.: carried out the X-ray diffraction. P.D.: supervised optoacoustic characterization. A.L.B., D.F., and M.G.: supervised the project, finalized the manuscript, and secured funding. M.G.: conceived, led, and coordinated the entire project, cowrote the manuscript, and secured funding. All of the authors contributed to the discussion of the results and approved the final version of the manuscript.

Notes

The authors declare no competing financial interest.

■ REFERENCES

(1) Ashby, M. F.; Greer, A. L. Metallic glasses as structural materials. *Scripta Materialia* **2006**, *54* (3), 321.

(2) Greer, A.; Cheng, Y.; Ma, E. Shear bands in metallic glasses. *Materials Science and Engineering: R: Reports* **2013**, *74* (4), 71−132.

(3) Nomoto, K.; Ceguerra, A. V.; Gammer, C.; Li, B.; Bilal, H.; Hohenwarter, A.; Gludovatz, B.; Eckert, J.; Ringer, S. P.; Kruzic, J. J. Medium-range order dictates local hardness in bulk metallic glasses. *Mater. Today* **2021**, *44*, 48−57.

(4) Nomoto, K.; Li, B.; Gammer, C.; Ceguerra, A. V.; Bilal, H.; Hohenwarter, A.; Eckert, J.; Gludovatz, B.; Ringer, S. P.; Kruzic, J. J. Deformation-induced medium-range order changes in bulk metallic glasses. *Phys. Rev. Mater.* **2022**, *6* (4), No. 043603.

(5) Ivanisenko, Y.; Kübel, C.; Nandam, S. H.; Wang, C.; Mu, X.; Adjaoud, O.; Albe, K.; Hahn, H. Structure and properties of nanoglasses. *Adv. Eng. Mater.* **2018**, *20* (12), No. 1800404.

(6) Nandam, S. H.; Schwaiger, R.; Kobler, A.; Kübel, C.; Wang, C.; Ivanisenko, Y.; Hahn, H. Controlling shear band instability by nanoscale heterogeneities in metallic nanoglasses. *J. Mater. Res.* **2021**, *36* (14), 2903−2914.

(7) Ghidelli, M.; Orekhov, A.; Bassi, A. L.; Terraneo, G.; Djemia, P.; Abadias, G.; Nord, M.; Beche, A.; Gauquelin, N.; Verbeeck, J.; Raskin, J.-P.; Schryvers, D.; Pardoen, T.; Idrissi, H. Novel class of nanostructured metallic glass films with superior and tunable mechanical properties. *Acta Mater.* **2021**, *213*, No. 116955.

(8) Ghidelli, M.; Idrissi, H.; Gravier, S.; Blandin, J.-J.; Raskin, J.-P.; Schryvers, D.; Pardoen, T. Homogeneous flow and size dependent mechanical behavior in highly ductile Zr65Ni35 metallic glass films. *Acta Mater.* **2017**, *131*, 246−259.

(9) Zhang, J.; Liu, G.; Lei, S.; Niu, J.; Sun, J. Transition from homogeneous-like to shear-band deformation in nanolayered crystalline Cu/amorphous Cu−Zr micropillars: Intrinsic vs. extrinsic size effect. *Acta Mater.* **2012**, *60* (20), 7183−7196.

(10) Guo, W.; Jägle, E.; Yao, J.; Maier, V.; Korte-Kerzel, S.; Schneider, J. M.; Raabe, D. Intrinsic and extrinsic size effects in the deformation of amorphous CuZr/nanocrystalline Cu nanolaminates. *Acta Mater.* **2014**, *80*, 94−106.

(11) Nasim, M.; Li, Y.; Wen, C. Length-scale dependent deformation, strengthening, and ductility of fcc/fcc Ni/Al nano-laminates using micropillar compression testing. *Acta Mater.* **2020**, *193*, 318−328.

(12) Cheng, B.; Trelewicz, J. R. Design of crystalline-amorphous nanolaminates using deformation mechanism maps. *Acta Mater.* **2018**, *153*, 314−326.

(13) Poltronieri, C.; Brognara, A.; Bignoli, F.; Evertz, S.; Djemia, P.; Faurie, D.; Challali, F.; Li, C.; Belliard, L.; Dehm, G.; Best, J. P.; Ghidelli, M. Mechanical properties and thermal stability of ZrCuAlx thin film metallic glasses: Experiments and first-principle calculations. *Acta Mater.* **2023**, *258*, No. 119226.

(14) Brognara, A.; Best, J. P.; Djemia, P.; Faurie, D.; Dehm, G.; Ghidelli, M. Effect of composition and nanostructure on the mechanical properties and thermal stability of Zr100-xCux thin film metallic glasses. *Mater. Design* **2022**, *219*, No. 110752.

(15) Oliver, W. C.; Pharr, G. M. An improved technique for determining hardness and elastic modulus using load and displacement sensing indentation experiments. *J. Mater. Res.* **1992**, *7* (6), 1564−1583.

(16) Guo, H.; Yan, P. F.; Wang, Y. B.; Tan, J.; Zhang, Z. F.; Sui, M. L.; Ma, E. Tensile ductility and necking of metallic glass. *Nat. Mater.* **2007**, *6* (10), 735−739.

(17) Wang, X.; Jiang, F.; Hahn, H.; Li, J.; Gleiter, H.; Sun, J.; Fang, J. Sample size effects on strength and deformation mechanism of Sc75Fe25 nanoglass and metallic glass. *Scripta Mater.* **2016**, *116*, 95−99.

(18) Ghidelli, M.; Gravier, S.; Blandin, J.-J.; Raskin, J.-P.; Lani, F.; Pardoen, T. Size-dependent failure mechanisms in ZrNi thin metallic glass films. *Scripta Mater.* **2014**, *89*, 9−12.

(19) Nandam, S. H.; Ivanisenko, Y.; Schwaiger, R.; Śniadecki, Z.; Mu, X.; Wang, D.; Chellali, R.; Boll, T.; Kilmametov, A.; Bergfeldt, T.; et al. Cu-Zr nanoglasses: Atomic structure, thermal stability and indentation properties. *Acta Mater.* **2017**, *136*, 181−189.

(20) Chen, Z. Q.; Li, M. C.; Cao, J. S.; Li, F. C.; Guo, S. W.; Sun, B. A.; Ke, H. B.; Wang, W. H. Interface dominated deformation transition from inhomogeneous to apparent homogeneous mode in amorphous/amorphous nanolaminates. *J. Mater. Sci. Technol.* **2022**, *99*, 178−183.

(21) Bhattacharyya, D.; Mara, N.; Dickerson, P.; Hoagland, R.; Misra, A. Compressive flow behavior of Al−TiN multilayers at nanometer scale layer thickness. *Acta Mater.* **2011**, *59* (10), 3804−3816.

(22) Aziz, M. J. Film growth mechanisms in pulsed laser deposition. *Appl. Phys. A: Mater. Sci. Process.* **2008**, *93*, 579−587.

(23) Takeuchi, A.; Inoue, A. Classification of bulk metallic glasses by atomic size difference, heat of mixing and period of constituent elements and its application to characterization of the main alloying element. *Mater. Trans.* **2005**, *46* (12), 2817−2829.

(24) Cui, Y.; Huang, P.; Wang, F.; Lu, T.; Xu, K. The hardness and related deformation mechanisms in nanoscale crystalline−amorphous multilayers. *Thin solid films* **2015**, *584*, 270−276.

(25) Schuh, C. A.; Lu, K. Stability of nanocrystalline metals: The role of grain-boundary chemistry and structure. *MRS Bull.* **2021**, *46*, 225−235.

(26) Zhang, Y.; Su, R.; Niu, T.; Richter, N.; Xue, S.; Li, Q.; Ding, J.; Yang, B.; Wang, H.; Zhang, X. Thermal stability and deformability of annealed nanotwinned Al/Ti multilayers. *Scripta Mater.* **2020**, *186*, 219−224.

(27) Yu, P.; Bai, H. Y. Poisson's ratio and plasticity in CuZrAl bulk metallic glasses. *Mater. Sci. Eng., A* **2008**, *485* (1−2), 1−4.

(28) Afonso, C. N.; Gonzalo, J. Pulsed laser deposition of thin films for optical applications. *Nucl. Instrum. Meth. B* **1996**, *116* (1−4), 404−409.

(29) Apakina, V.; Karuzskii, A.; Kogan, M.; Kvit, A.; Melnik, N.; Mityagin, Y. A.; Murzin, V.; Orlikovsky, A.; Perestoronin, A.; Tkachenko, S.; et al. Studies of nanoscale structure and its transformation in pulsed-laser deposited dense diamond-like carbon films. *Diam. Relat. Mater.* **1997**, *6* (5−7), 564−568.

(30) Anderson, K.; Weritz, J.; Kaufman, J. G. 1xxx Aluminum Alloy Datasheets. In *Properties and Selection of Aluminum Alloys, ASM Handbooks*, Vol. *2B*; ASM International, 2019; pp 1..

(31) Oliver, W. C.; Pharr, G. M. Measurement of hardness and elastic modulus by instrumented indentation: Advances in understanding and refinements to methodology. *J. Mater. Res.* **2004**, *19* (1), 3−20.

(32) Apreutesei, M.; Steyer, P.; Joly-Pottuz, L.; Billard, A.; Qiao, J.; Cardinal, S.; Sanchette, F.; Pelletier, J. M.; Esnouf, C. Microstructural, thermal and mechanical behavior of co-sputtered binary Zr−Cu thin film metallic glasses. *Thin solid films* **2014**, *561*, 53−59.

(33) Besozzi, E.; Dellasega, D.; Pezzoli, A.; Conti, C.; Passoni, M.; Beghi, M. Amorphous, ultra-nano-and nano-crystalline tungsten-based coatings grown by Pulsed Laser Deposition: mechanical characterization by Surface Brillouin Spectroscopy. *Mater. Design* **2016**, *106*, 14−21.

(34) Besozzi, E.; Dellasega, D.; Russo, V.; Conti, C.; Passoni, M.; Beghi, M. G. Thermomechanical properties of amorphous metallic tungsten-oxygen and tungsten-oxide coatings. *Mater. Design* **2019**, *165*, No. 107565.

(35) Xue, F.; Huang, P.; Liu, M.; Xu, K.; Wang, F.; Lu, T. Unusual strain rate sensitivity of nanoscale amorphous CuZr/crystalline Cu multilayers. *Mater. Sci. Eng., A* **2017**, *684*, 84−89.

(36) Kuan, S.; Du, X.; Chou, H.; Huang, J. Mechanical response of amorphous ZrCuTi/PdCuSi nanolaminates under nanoindentation. *Surf. Coat. Technol.* **2011**, *206* (6), 1116−1119.

(37) Das, J.; Tang, M. B.; Kim, K. B.; Theissmann, R.; Baier, F.; Wang, W. H.; Eckert, J. Work-hardenable" ductile bulk metallic glass. *Phys. Rev. Lett.* **2005**, *94* (20), No. 205501.

(38) Farhat, Z.; Ding, Y.; Northwood, D.; Alpas, A. Effect of grain size on friction and wear of nanocrystalline aluminum. *Mater. Sci. Eng., A* **1996**, *206* (2), 302−313.

(39) Liu, M.; Du, X.; Lin, I.; Pei, H.; Huang, J. Superplastic-like deformation in metallic amorphous/crystalline nanolayered micropillars. *Intermetallics* **2012**, *30*, 30−34.

(40) Wu, G.; Liu, C.; Sun, L.; Wang, Q.; Sun, B.; Han, B.; Kai, J.-J.; Luan, J.; Liu, C. T.; Cao, K.; et al. Hierarchical nanostructured aluminum alloy with ultrahigh strength and large plasticity. *Nat. Commun.* **2019**, *10* (1), 5099.

(41) Ye, J.; Chu, J.; Chen, Y.; Wang, Q.; Yang, Y. Hardness, yield strength, and plastic flow in thin film metallic-glass. *J. Appl. Phys.* **2012**, *112* (5), 053516.

(42) Wu, G.; Chan, K.-C.; Zhu, L.; Sun, L.; Lu, J. Dual-phase nanostructuring as a route to high-strength magnesium alloys. *Nature* **2017**, *545* (7652), 80−83.

(43) Ritter, Y.; Şopu, D.; Gleiter, H.; Albe, K. Structure, stability and mechanical properties of internal interfaces in Cu64Zr36 nanoglasses studied by MD simulations. *Acta Mater.* **2011**, *59* (17), 6588−6593.

(44) Şopu, D.; Ritter, Y.; Gleiter, H.; Albe, K. Deformation behavior of bulk and nanostructured metallic glasses studied via molecular dynamics simulations. *Phys. Rev. B* **2011**, *83* (10), No. 100202.

(45) Wu, G.; Liu, C.; Brognara, A.; Ghidelli, M.; Bao, Y.; Liu, S.; Wu, X.; Xia, W.; Zhao, H.; Rao, J.; et al. Symbiotic crystal-glass alloys via dynamic chemical partitioning. *Mater. Today* **2021**, *51*, 6−14.

(46) Johnson, W.; Samwer, K. A universal criterion for plastic yielding of metallic glasses with a (T/T g) 2/3 temperature dependence. *Phys. Rev. Lett.* **2005**, *95* (19), No. 195501.

(47) Chou, H.; Du, X.; Lee, C.; Huang, J. Enhanced mechanical properties of multilayered micropillars of amorphous ZrCuTi and nanocrystalline Ta layers. *Intermetallics* **2011**, *19* (7), 1047−1051.

(48) Raghavan, R.; Wheeler, J.; Esqué-De los Ojos, D.; Thomas, K.; Almandoz, E.; Fuentes, G.; Michler, J. Mechanical behavior of Cu/TiN multilayers at ambient and elevated temperatures: Stress-assisted diffusion of Cu. *Mater. Sci. Eng., A* **2015**, *620*, 375−382.

(49) Ashby, M.; Greer, A. L. Metallic glasses as structural materials. *Scripta Mater.* **2006**, *54* (3), 321−326.